

# Hybrid Pixel-Unshuffled Network for Lightweight Image Super-Resolution

Bin Sun<sup>1,3</sup>, Yulun Zhang<sup>2</sup>, Songyao Jiang<sup>4</sup>, and Yun Fu<sup>1,3</sup>

<sup>1</sup> Northeastern University, Boston, MA, USA

<sup>2</sup> ETH Zürich, Zürich, Switzerland

<sup>3</sup> AInnovation Labs Inc., Boston, MA, USA

<sup>4</sup> Amazon Lab126, Sunnyvale, CA, USA

**Abstract.** Convolutional neural network (CNN) has achieved great success on image super-resolution (SR). However, most deep CNN-based SR models take massive computations to obtain high performance. Downsampling features for multi-resolution fusion is an efficient and effective way to improve the performance of visual recognition. Still, it is counter-intuitive in the SR task, which needs to project a low-resolution input to high-resolution. In this paper, we propose a novel Hybrid Pixel-Unshuffled Network (HPUN) by introducing an efficient and effective downsampling module into the SR task. The network contains pixel-unshuffled downsampling and Self-Residual Depthwise Separable Convolutions. Specifically, we utilize pixel-unshuffle operation to downsample the input features and use grouped convolution to reduce the channels. Besides, we enhance the depthwise convolution’s performance by adding the input feature to its output. Experiments on benchmark datasets show that our HPUN achieves and surpasses the state-of-the-art reconstruction performance with fewer parameters and computation costs.

**Keywords:** Super Resolution, Down-sample, Pixel-unshuffle, Lightweight

## 1 Introduction

Single Image Super-Resolution (SISR) is a fundamental vision task to reconstruct a faithful high-resolution (HR) image from a low-resolution (LR) image. SISR has been utilized on various high-level tasks such as face synthesis [53,52], medical imaging [39], surveillance imaging [64], and image generation [22]. Dong *et al.* [5] first introduced CNN into SISR and achieved impressive performance in 2014. Afterwards, more deep CNN methods are proposed for the super-resolution tasks [37,15,23,24,29,46,43,58,60]. Among these, one of the most fundamental architectures is EDSR [29]. However, these networks need expensive computation resources, which is the main bottleneck for their deployment on mobile devices.

In recent years, a lot of manually designed lightweight structures have been proposed [40,13,4,18,36,59,32,12,21,9]. Among these structures, the most fundamental one is the depthwise convolution layer [40], which processes the spatial information with a single convolution on each input feature. A  $1 \times 1$  convolution

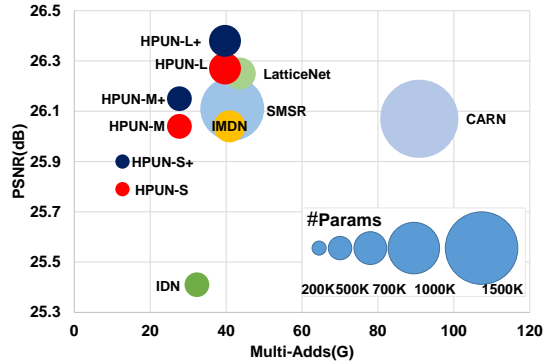


**Fig. 1.** Illustration of the overall comparison on Urban100 with  $\times 4$  scale. Our proposed HPUN-L achieves the best trade-off among the PSNR, parameters, and Multi-Adds. + means the PSNR results are generated with self-ensemble.

layer named pointwise layer is usually deployed around the depthwise convolution layer for the communication among channels [13,36,12,59,32]. However, such structures are not popular in the SISR due to their significant performance loss. CARN [1] tried to use a similar structure as MobileNet [13] on SISR in 2018. They utilized the group convolution to reduce the parameters, but they had to introduce a complicated recurrent scheme to improve the performance. As shown in Figure 1, the computation costs and parameters of CARN are not satisfied. Therefore, it is still a main challenge to effectively implement depthwise convolution based lightweight structures to the image super-resolution task.

Besides using lightweight operations, the computation costs can be alleviated by reducing the size of feature maps [44,13,4,18,36,59,32,12,21,9]. Meanwhile, size-reduced features can also improve high-level representations by merging with higher-resolution features in many tasks [41,47]. However, it is counter-intuitive to apply downsampling modules in SISR since SISR is an upsampling task that restores information of a low-resolution image. In contrast, the downsampling operation usually causes significant information loss. Haris *et al.* [11] proposed an iterative error-correcting feedback mechanism that calculates both up- and down-projection errors to guide the reconstruction. Furthermore, Li *et al.* [28] also proposed a framework that introduced the downsampling module into SISR to generate high-level representations. Their success shows the possibility of getting pleasing high-resolution images through downsampling operations. However, they still had to utilize a recurrent scheme to resist the performance drop, which heavily increased the parameters and computation costs.

This paper explores an effective way to design a lightweight network with depthwise convolutions and downsampling operations. Specifically, we develop a simple yet effective module named Self-Residual Depthwise Separable Convolution to overcome the drawback in Depthwise Separable Convolution (DSC) [13] without any additional parameters. Inspired by the previous explorations on downsampling features [41,11,28], we propose a pixel-unshuffled downsampler constructed with the pixel-unshuffle operation, max-pooling, and group convolution to further enhance the performance of DSC with similar computation costs

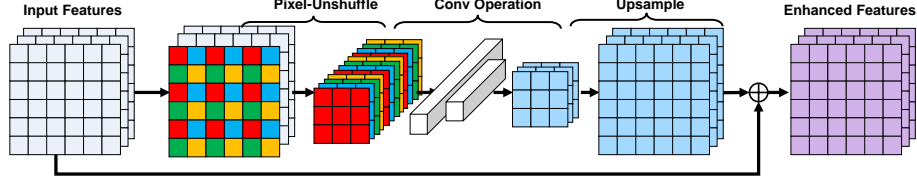


**Fig. 2.** The scheme of our proposed pixel-unshuffled downsampler. Note that the notation of Conv Operation in the figure is a general operation. We will explore the best operations in the following sections.

as depthwise convolution. The scheme is shown in Figure 2. The pixel-unshuffle operation is the reverse operation of pixel-shuffle [38]. Moreover, we propose a practical, lightweight module named Pixel-Unshuffled Block (PUB) constructed with the pixel-unshuffled downsampling and the Self-Residual DSC. Last, we replace one Self-Residual DSC in the PUB with a standard convolution layer and construct a Hybrid Pixel-Unshuffled Network (HPUN) to achieve the state-of-the-art (SOTA) performance and slightly increase the number of the HPUN to beyond the SOTA performance. The overall comparison is shown in Figure 1. The main contributions are summarized as:

- We propose the Self-Residual DSC to overcome the defects of the depthwise convolution in the SISR task with a simple and effective operation, which barely needs computation and additional parameters.
- We propose a novel downsampling module with the pixel-unshuffle operation, which is our key module to enhance the performance.
- We propose a lightweight module named PUB with our Self-Residual DSC and the pixel-unshuffled downsampler, which can provide reliable performance with a few parameters and computation costs.
- We propose the Hybrid Pixel-Unshuffled Block (HPUB) by integrating the standard convolution into the PUB, and construct the effective and efficient HPUN to achieve a new SOTA performance with a few parameters and Multi-Adds comparing the baselines.
- We discover the relationship between PSNR and the Normalized Mean Error (NME) among the shallow features and deep features based on our ablation study, which may be valuable in designing the network for SISR. We will discuss the details in section 4.2.

## 2 Related Work

### 2.1 Super Resolution

**Deep Super Resolution.** An end-to-end mapping between the interpolated LR images and their HR counterparts was first established by SRCNN [5]. The SRCNN was further improved by its successors with advanced network architectures [23, 57]. As studied in [7], computational costs are quadratically increased

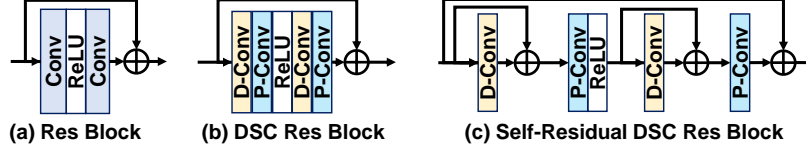


**Fig. 3.** Illustration of modules. (a) standard residual block. (b) the residual block constructed by depthwise separable convolution (DSC). (c) the residual block constructed by our proposed Self-Residual DSC. Abbrevs.: D-Conv=Depthwise Convolution, P-Conv=Pointwise Convolution.

by this upsampling operation in data preprocessing. To solve the problem, an efficient sub-pixel convolution layer that upsampled the last LR feature maps to HR was introduced in ESPCN [38]. It was also adopted in residual-learning networks SRResNet [27] and EDSR [29]. The performance of the SISR was then further improved by stacking more blocks with dense residuals [56,55,62,61].

**Lightweight Super Resolution.** LapSRN [26] reduced the computation complexity by removing the bicubic interpolation before prediction. Inspired by LapSRN, a lot of works started to reconstruct the HR image from the origin LR input. Recursive learning was first introduced by DRCN [24]. Then it was widely used to reduce the parameters with weight sharing strategy [42,43,11,1,28]. Besides the recurrent scheme, IDN [17] and CARN [1] introduced the group convolution for the lightweight purpose. As the success of the residual operation in SISR, many works [17,16,31] adopted the residual into their lightweight design to keep the performance. A recent work named SMSR [48] reduced the parameters and computation costs with pruning. Different with SMSR, we manually design the lightweight network which can be further improved by pruning.

## 2.2 Deep Lightweight Structure

In recent years, as the deep-learning models become deeper and larger, many researchers have been working on the lightweight networks. A faster activation function named rectified-linear activation function (ReLU) was proposed to accelerate the model in [8]. A flattened CNN architecture that accelerated the feeding forward was presented in [20]. Depthwise separable convolution was first proposed in [40] and was widely adopted in Inception models [19], Xception network [4], MobileNets [13,36], ShuffleNets [59,32] and CondenseNet [14]. Besides manually designed lightweight architectures, researchers proposed to use Neural Architecture Search (NAS) to find the optimal lightweight network [30,63,3,51,12,21]. All these networks are constructed based on the depthwise convolution as well. Thus, it is necessary to explore an effective way to implement the depthwise convolution on SISR. In this work, we propose a down-sampling module which can significantly enhance the performance based on the depthwise convolution.

### 3 Proposed Method

We propose a lightweight structure called Hybrid Pixel-Unshuffled Block to replace the traditional Residual Convolution Block, which is shown in Figure 3(a). Our proposed method has three parts: a standard convolution layer, the proposed pixel-unshuffled downsampling, and the proposed PUB. Specifically, the PUB is an integration of the pixel-unshuffled downsampling and the Self-Residual DSC. Therefore, we organize this section as follows: first, we will introduce the details of the Self-Residual DSC; the pixel-unshuffled downsampling will be introduced in the second sub-section; at last, we will present the details of the HPUN.

#### 3.1 Self-Residual DSC

**DSC.** Depthwise separable convolution (DSC) is composed by a depthwise layer and a pointwise layer as shown in Fig. 3(b). The depthwise layer uses single kernel for each input feature map. DSC is a popular lightweight module to reduce the redundant operations in the standard convolution. The conversion from the standard convolution to the DSC can be described as:

$$\mathbf{F}^{\text{out}} = C(\mathbf{F}^{\text{in}}) \approx P(D(\mathbf{F}^{\text{in}})), \quad (1)$$

where  $\mathbf{F}^{\text{out}}$  means the output features,  $C$  represents the standard convolution,  $\mathbf{F}^{\text{in}}$  means the input features,  $D$  means the depthwise convolution, and  $P$  means the pointwise convolution. Depthwise convolution is the major part to process the spatial information of the input features, which needs far fewer parameters and computation costs than the standard convolution.

**Self-Residual DSC.** It may have a significant side effect on the performance of SISR since SISR needs to enrich the information. The side effect is shown in section 4.2. To overcome the defects brought by the depthwise layer and keep its ability to process the spatial information, We find a balanced trade-off design by simply adding the input before the depthwise layer to the output of the depthwise layer as shown in Figure 3(c). The whole structure is described as:

$$\mathbf{F}^{\text{out}} = P(D(\mathbf{F}^{\text{in}}) + \mathbf{F}^{\text{in}}). \quad (2)$$

Comparing Equation (1) and Equation (2), we can easily figure out that the outputs of the Self-Residual DSC have more similarity to the inputs than the outputs of the DSC. We will analyze the importance of the similarity in section 4.2. The self-residual does not introduce any additional parameters. Besides, the additional computation costs of addition operation can be ignored.

#### 3.2 Pixel-Unshuffled Downsampling

Now we present details about the pixel-unshuffled downsampling, which is shown in Figure 4(a). As discussed in previous sections, low-frequency features can enhance the high-level representations [41,47]. In the work [47], it is explored that repeating multi-resolution fusions can boost the high-resolution representations with the help of the low-resolution representations in image segmentation tasks. However, previous SR works [11,28] took a lot of effort to use the low-frequency

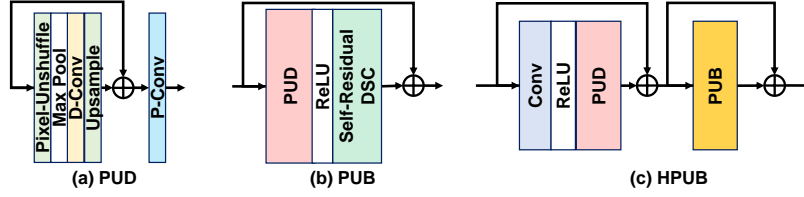


**Fig. 4.** (a) Pixel-Unshuffled Downsampling (PUD). (b) Pixel-Unshuffled Block (PUB). (c) Hybrid Pixel-Unshuffled Block (HPUB). Note that the group number of the depth-wise convolution in the PUD equals to the number of its inputs.

features in SISR with a heavy recurrent scheme. In this work, we explore a more efficient way to utilize the low-frequency features with single forward inference for the SISR task. The proposed scheme is shown in Figure 2. In this subsection, we will first introduce the pixel-unshuffle operation. Then we will focus on exploring the most effective operations after the pixel-unshuffle.

**Pixel-unshuffle.** Pixel-unshuffle is a reverse operation of pixel-shuffle [38]. As shown in Figure 2, it divides a feature into several sub-features, whose number in this work is four. We use four different color to represent sub-features in the figure. As shown in the figure, the sub-features contain the complete information of the original features but with lower resolution. Therefore, we use it to avoid information loss while reducing the size of the features.

**Pixel-Unshuffled Downsampling.** After the pixel-unshuffle operation, we need a efficient and effective structure to process the low-resolution features. As shown in Figure 4(a), we first deploy a max-pooling after the pixel-unshuffle. The reason is we want a powerful non-linear operation before the convolution operation to extract better local features. Therefore, we choose the max-pooling instead of the average-pooling layer. We describe the process as:

$$F_{i,j}^{\text{out}} = M(F_{i,j}^{\text{in}}), \quad i \in \{1, 2, 3, 4\}, j \in \{1 \dots n\}, \quad (3)$$

where  $F_{i,j}^{\text{in}}$  means the  $i$ th sub-feature of  $j$ th input channel,  $F_{i,j}^{\text{out}}$  means the  $i$ th sub-feature of  $j$ th output channel, and  $M$  means max-pooling with stride 1.

After the non-linear operation, we use a group convolution to reduce the channel of the input, which is actually a downsampling operation. The process can be described as:

$$F_j^{\text{out}} = G(F_{1,j}^{\text{in}}, F_{2,j}^{\text{in}}, F_{3,j}^{\text{in}}, F_{4,j}^{\text{in}}), \quad j \in \{1 \dots n\}, \quad (4)$$

where  $F_j^{\text{out}}$  means the  $j$ th output channel, and  $G$  means the grouped convolution whose group number equals to 4.

To enhance the feature, we use an upsampler to project the low-frequency features to high dimension, and add them to the original input features. After that, a pointwise convolution is utilized for the communication among the channels. The process can be described as:

$$\mathbf{F}^{\text{out}} = P(U(\mathbf{F}^{\text{in}}) + \mathbf{L}), \quad (5)$$

where  $U$  stands for the upsampling function,  $\mathbf{F}^{\text{in}}$  means the input channels to the upsampler, and  $\mathbf{L}$  means the original input features. We use bi-linear upsampler. The experiments will be shown in section 4.2.

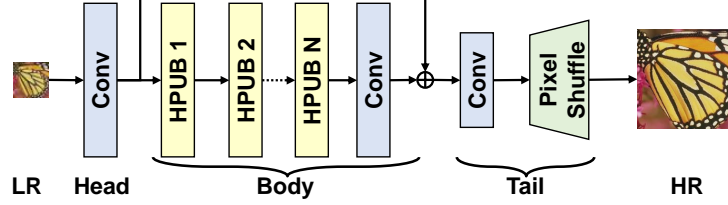


**Fig. 5.** Our proposed HPUN. The architecture is based on EDSR, and the tail is from IMDN. The total number of HPUBs in HPUN is no less than 8.

### 3.3 Hybrid Pixel-Unshuffled Network

**Pixel-Unshuffled Block.** After the exploration of the Self-Residual DSC and the pixel-unshuffled downsampling, we introduce the lightweight Pixel-Unshuffled Block (PUB). The PUB is composed of the Self-Residual DSC and the pixel-unshuffled downsampling. The detail of PUB is shown in Figure 4(b). The block can be represented as:

$$\mathbf{F}^{\text{out}} = P(D(\sigma(\text{PUD}(\mathbf{F}^{\text{in}}))) + \sigma(\text{PUD}(\mathbf{F}^{\text{in}}))) + \mathbf{F}^{\text{in}}, \quad (6)$$

where the PUD denotes the whole procedure of the pixel-unshuffled downsampling, and  $\sigma$  represents the ReLU [8].

**Hybrid Pixel-Unshuffled Block.** To further improve the performance, we integrate the standard convolution into our proposed PUB, which is named as Hybrid Pixel-Unshuffled Block (HPUB). The details of the HPUB are shown in Figure 4(c). The kernel size of the standard convolution layer is set to 3 for the trade-off between the performance and the efficiency. The kernel setting of the rest modules is the same as the PUB, which will be demonstrated in section 4.2.

**Hybrid Pixel-Unshuffled Network.** We use HPUB to construct our Hybrid Pixel-Unshuffled Network (HPUN). The network is similar to EDSR. Since one HPUB has two residual blocks, we construct the body parts with 8 HPUB to align the settings in EDSR. To further reduce the parameters, we use the tail of IMDN. The details of the architecture are shown in Figure 5. We control the total number of HPUB for different sizes of the model. HPUN-M has 8 HPUN blocks in total, and HPUN-L has 12 HPUN blocks. The total number of HPUN-S is 8, but we replace one HPUB with two PUBs. The upsampler for the final high-resolution output is the pixel-shuffle module [38].

## 4 Experimental Results

### 4.1 Settings

**Datasets and Metrics.** Following [10,45,29,58], we use dataset DIV2K [45] and Flickr2K [29] as training data. We use five standard benchmark datasets as testing: Set5 [2], Set14 [54], B100 [33], Urban100 [15], and Manga109 [34]. The SR results are evaluated with PSNR and SSIM [50] on Y channel (*i.e.* luminance) of transformed YCbCr space. Following the work [58,61], the degradation is bicubic

downsampling by adopting the Matlab function *imresize* with the option *bicubic* (denote as **BI** for short). We use **BI** model to simulate LR images with scaling factor  $\times 2$ ,  $\times 3$ , and  $\times 4$ . We also compare the parameters and Multi-Adds to evaluate the spatial and time complexity.

**Training Setting.** Following settings of [29], in each training batch, we randomly extract 16 LR RGB patches with the size of  $48 \times 48$  as inputs. We randomly augment the patches by flipping horizontally or vertically and rotating  $90^\circ$ . There are 14,200 iterations in one epoch. We implement our HPUN with the PyTorch [35] and update it with Adam optimizer [25]. The learning rate is initialized to  $2 \times 10^{-4}$  for all layers and follows the cosine scheduler with 250 epochs in each cycle. Some experiments use the step scheduler and will be emphasized in the caption for fair comparison.

## 4.2 Ablation Study

We first demonstrate the effectiveness of the Self-Residual DSC. Then we will show the enhancement of the pixel-unshuffled downsampling. A set of experiments are implemented to figure out the best operation in the pixel-unshuffled downsampling. Besides, we will also explore the best setting of kernel size in the PUB. At last, we will visualize the features and discuss our intuition.

**Table 1.** Experiment results of different components in DSC generated with step schedule. Conv represents standard convolution.

Methods	PSNR(Set5)	Params	Multi-Adds
Conv Res-Block	38.05	1343K	309.9G
Conv+DSC	37.88	701K	163.6G
Conv+P-Conv	37.90	690K	161.5G
Conv+Self-Residual DSC	37.91	701K	163.6G
DSC only	37.65	207K	44.9G
P-Conv only	37.36	181K	40.7G
Self-Residual DSC only	37.73	207K	44.9G

**Effectiveness of the Self-Residual DSC.** From the Table 1, we can find out that the combination of standard convolution and DSC gets worse PSNR than the combination of standard convolution and the pointwise convolution. Therefore, we can draw a conclusion that the depthwise convolution will obstruct the accuracy of the image reconstruction in the DSC. However, we cannot abandon the depthwise convolution when we design the lightweight network without standard convolution. The results presented in Table 1 and Figure 6 show that our Self-Residual DSC can overcome the defects of the depthwise convolution with a simple residual with barely no additional computation costs and parameters.

**Effectiveness of the pixel-unshuffled downsampling.** We have run six experiments to find the best combination of the pooling layer and the upsampler. The results are shown in Table 2. From the table, we can find out that the model with max-pooling layer and bi-linear upsampling can achieve the best performance among all combinations.



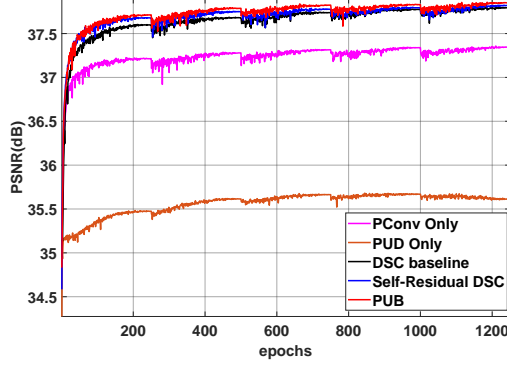


**Fig. 6.** Comparison among the networks constructed by pointwise convolution, pixel-unshuffled downsampling, baseline, DSC, the Self-Residual DSC, and the PUB. PUB stands for pixel-unshuffled downsampling. The experiment results of different combination of pooling layers and upsamplers. The results are generated with cosine scheduler on Set5 with  $\times 2$  scale.

Nearest	×	✓	✓	×	✓	×
Bi-linear	✓	×	×	✓	×	✓
Max-pooling	×	×	×	✓	×	×
Avg-pooling	✓	✓	×	×	×	×
PSNR	37.83	37.82	37.85	37.87	37.82	37.83

We also compare the performance of the pixel-unshuffled downsampling with other kinds of downsampling operations. The results are shown in Figure 7(a). We compare the PUD module, depthwise convolution with 2 strides, max pooling, and average pooling with both bi-linear and nearest upsampling. As shown in the figure, the pixel-unshuffled downsampling is far beyond others.

Besides, we construct a network with only pixel-unshuffled downsampling and compare its performance with the networks constructed by the baseline DSC, the Self-Residual DSC, and the PUB. The results are shown in Figure 6. The network constructed with only pixel-unshuffled downsampling performs far worse than the baseline DSC. However, the network of PUB can performs better than the Self-Residual DSC. Specifically, the network constructed by PUB achieves 0.04dB higher than the Self-Residual DSC only. The results show that the pixel-unshuffled downsampling can enhance the performance, but it only works together with other spatial operations.

**Ablation Study of the PUB.** We run some experiments to explore the impact brought by different settings of kernels. The results are shown in Figure 7(b). We compare the performance among the setting  $1-3-1-3$ ,  $1-5-1-5$ ,  $3-3-3-3$ ,  $3-5-3-5$ ,  $1-3-3-3$ , and  $1-3-3-5$ . From the figure, we can find the setting  $1-3-3-5$  performs superior to all other settings. Therefore, we use  $1-3-3-5$  as the kernel settings of the PUB.

**Intuition.** For the further exploration, we generate the heatmap features using the Normalized Mean Error (NME) among their head features and body features. The NME can be described as  $NME = \frac{1}{N} \|\mathbf{F}^H - \mathbf{F}^B\|_F$ , where  $N$  means the total

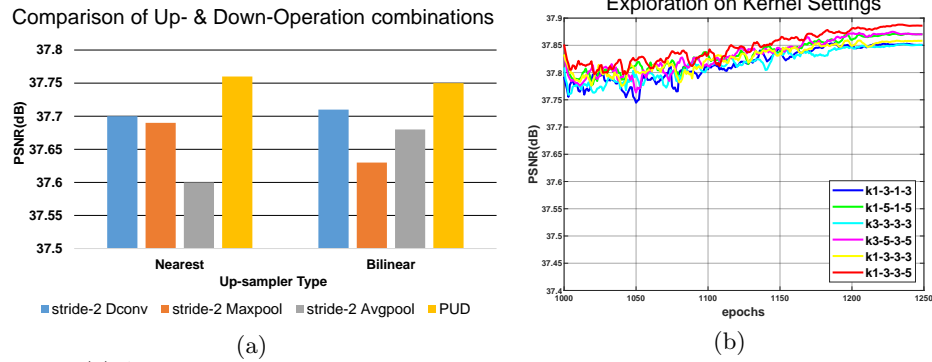


**Fig. 7.** (a): An ablation study of different combinations of up- and down-scale operations. The results are conducted with step scheduler and should not be compared with our other experiments. (b): We explore different settings on kernels of depthwise layer in the PUB. The PSNR is calculated on Set5 with  $\times 2$  scale.

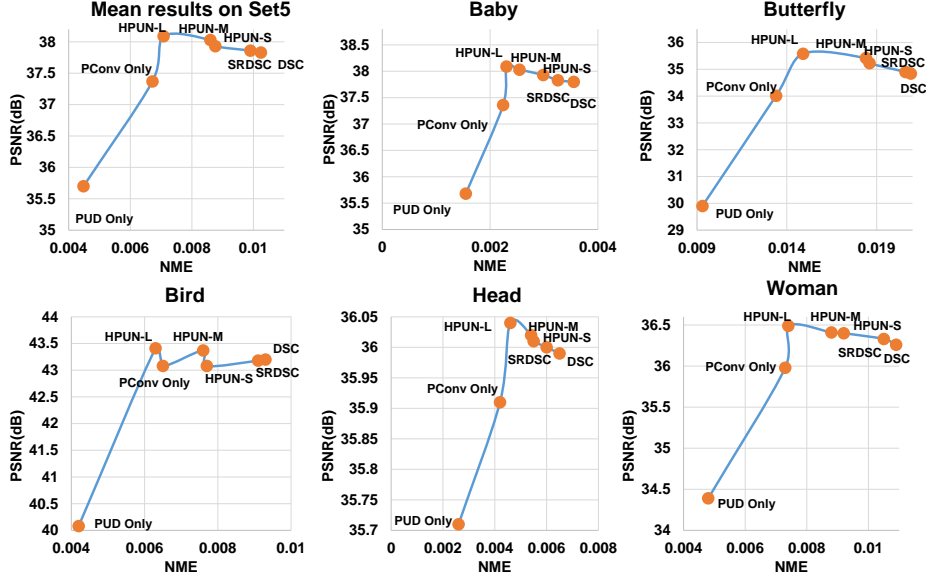


**Fig. 8.** Charts of the relationship between PSNR and the NME. The upper-left chart is generated on the whole Set5 dataset with  $\times 2$  scale. The rest results are generated for the image in the Set5 respectively. Abbrevs.: PUD=Pixel-Unshuffled Downsampling, SRDSC=Self-Residual DSC.

number of the elements in the features,  $\mathbf{F}^H$  means the output features from the head block,  $\mathbf{F}^B$  means the output features from the body block, and  $\|\cdot\|_F$  denotes the Frobenius norm. We plot the relationship between the PSNR and NME for the network constructed with pointwise convolutions, the network with DSC, the network with Self-Residual DSC, the network with pixel-unshuffled downsampling, HPUN-S, HPUN-M, and HPUN-L. The results are presented in Figure 8. We also show the result of single image besides the mean results.

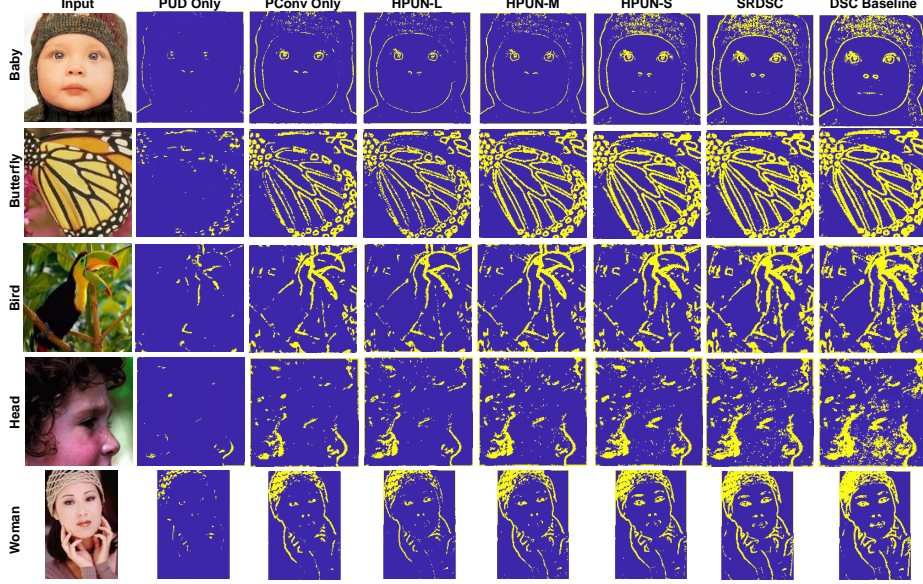


**Fig. 9.** The NME visualization of Pointwise Convolution, DSC, Self-Residual DSC, pixel-unshuffled downsampling, HPUN-S, HPUN-M, and HPUN-L. The results are generated on Set5 dataset with  $\times 2$  scale. The brighter color means the higher NME value. We binarize the features for better visualization. Abbrevs.: PUD=Pixel-Unshuffled Downsampling, SRDSC=Self-Residual DSC. Better view in color.

From the figure, we can find out that the NME of the pointwise structured network is much lower than the DSC baseline network, which means the main change of the features is brought by the depthwise convolution. The PSNR results of the pointwise structured network and pixel-unshuffled downsampler structured network show that limited changes will decrease the performance. However, the DSC network has large NME but limited PSNR, which means the larger NME does not represent the better performance. Although the chart generated from the bird indicate that there exist some variance, the conclusion still stands. We also visualize the NME result among the head features and body features of these networks, respectively. The visualization results are shown in Figure 9.

Thus, we can conclude that **the PUD can significantly reduce the NME among the shallow features and deep features**. Adjusting the number of the modules will improve the performance of the architecture. Besides, we find out that the NME among the head and body features gets smaller when we integrate the standard convolution into the PUB comparing the heatmap features of HPUN-S and HPUN-M. Considering the NME of the pointwise structured network, it is natural to think about the communication among the features can also help to learn the similarity among the features.

From the scatter figure of mean results, we notice that the performance increases explosively with the increase of the NME at first. Then the performance starts to drop after the NME surpasses the value around 0.007. Besides, the NME gets smaller by increasing the number of pixel-unshuffled downsamplers.

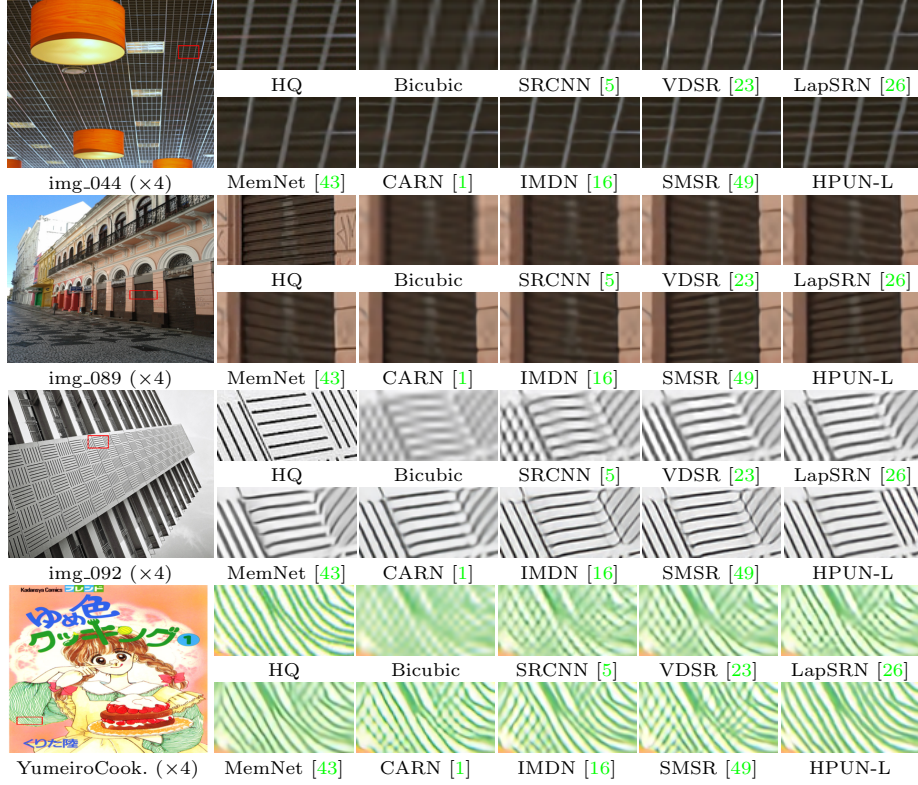


**Fig. 10.** Visual comparison with lightweight SR networks on Urban100 and Manga109.

Therefore, we can conclude that there may exist an optimal NME value, and increasing pixel-unshuffled downsamplers or adding residuals will reduce the NME of the network towards the optimal. The intuition can help us to design the network structure or apply the pruning strategy on SISR. However, we notice that the optimal NME is variable with the inputs. We still need more experiments to validate the conclusion for different tail structures and datasets in the future.

### 4.3 Comparison Results

Simulating LR image with BI degradation model is widely used in image SR settings. For BI degradation model, we compare our HPUN network with 12 state-of-the-art SR methods: SRCNN [6], VDSR [23], DRCN [24], DRRN [42], LapSRN [26], MemNet [43], CARN [1], IDN [17], SRFBN-S [28], IMDN [16], LatticeNet [31], and SMSR [48]. All of them are popular lightweight SR methods.

**Quantitative Results.** Quantitative results are shown in Table 3 for  $\times 2$ ,  $\times 3$ , and  $\times 4$  SR. Among all methods, our HPUN-L achieves the new SOTA performance on every dataset with the scale of  $\times 3$  and  $\times 4$ . When the scale is  $\times 2$ , our HPUN-L network still achieves the best performance on Set14, B100, and Manga109. Its PSNR on Urban100 is a little lower than LatticeNet, but its SSIM

**Table 3.** Benchmark results with **BI** degradation model. Average PSNR & SSIM values for scaling factor  $\times 2$ ,  $\times 3$ , and  $\times 4$ . We highlight the top-2 least params, Multi-Adds, and performance on each datasets with **bold red** (best) and underlined blue (second), respectively. + denotes the results are generated with self-ensemble.

Method Name	Scale	Params	Multi-Adds	Set5		Set14		B100		Urban100		Manga109	
				PSNR	SSIM	PSNR	SSIM	PSNR	SSIM	PSNR	SSIM	PSNR	SSIM
Bicubic	$\times 2$	-	-	33.66	0.9299	30.24	0.8488	29.56	0.8431	26.88	0.8403	30.80	0.9339
SRCNN[6]	$\times 2$	<b>57K</b>	52.7G	36.66	0.9542	32.45	0.9067	31.36	0.8879	29.50	0.8946	35.60	0.9663
VDNR[23]	$\times 2$	665K	612.6G	37.53	0.9590	33.05	0.9130	31.90	0.8960	30.77	0.9140	37.22	0.9750
DRCN[24]	$\times 2$	1774K	9788.7G	37.63	0.9588	33.04	0.9118	31.85	0.8942	30.75	0.9133	37.55	0.9732
DRRN[42]	$\times 2$	297K	6797.0G	37.74	0.9591	33.23	0.9136	32.05	0.8973	31.23	0.9188	37.92	0.9760
LapSRN[26]	$\times 2$	813K	<b>29.9G</b>	37.52	0.9591	33.08	0.9130	31.08	0.8950	30.41	0.9101	37.27	0.9740
MemNet[43]	$\times 2$	677K	623.9G	37.78	0.9597	33.28	0.9142	32.08	0.8978	31.31	0.9195	37.72	0.9740
CARN[1]	$\times 2$	1592K	222.8G	37.76	0.9590	33.52	0.9166	32.09	0.8978	31.92	0.9256	38.36	0.9765
IDN[17]	$\times 2$	553K	127.7G	37.83	0.9600	33.30	0.9148	32.08	0.8985	31.27	0.9196	38.01	0.9749
SRFBN-S[28]	$\times 2$	282K	574.4G	37.78	0.9597	33.35	0.9156	32.00	0.8970	31.41	0.9207	38.06	0.9757
IMDN[16]	$\times 2$	694K	158.8G	38.00	0.9605	33.63	0.9177	32.19	0.8996	32.17	0.9283	38.88	0.9774
LatticeNet[31]	$\times 2$	756K	169.5G	<b>38.15</b>	<b>0.9610</b>	33.78	0.9193	32.25	0.9005	<u>32.43</u>	0.9302	-	-
SMSR[48]	$\times 2$	985K	131.6G	38.00	0.9601	33.64	0.9179	32.17	0.8990	32.19	0.9284	38.76	0.9771
HPUN-S	$\times 2$	<u>226K</u>	<u>45.9G</u>	37.93	0.9604	33.46	0.9170	32.13	0.8990	31.70	0.9245	38.60	0.9768
HPUN-M	$\times 2$	492K	106.2G	38.03	0.9604	33.60	0.9185	32.20	0.9000	32.09	0.9282	38.83	0.9775
HPUN-L	$\times 2$	714K	151.1G	<b>38.09</b>	<b>0.9608</b>	<b>33.79</b>	<b>0.9198</b>	<b>32.25</b>	<b>0.9006</b>	<u>32.37</u>	<b>0.9307</b>	<b>39.07</b>	<b>0.9779</b>
HPUN-S+	$\times 2$	<u>226K</u>	<u>45.9G</u>	38.01	0.9605	33.54	0.9177	32.17	0.8994	31.84	0.9257	38.82	0.9774
HPUN-M+	$\times 2$	492K	106.2G	38.08	0.9607	33.67	0.9190	32.24	0.9004	32.23	0.9294	39.03	0.9779
HPUN-L+	$\times 2$	714K	151.1G	<b>38.15</b>	<b>0.9610</b>	<b>33.87</b>	<b>0.9206</b>	<b>32.29</b>	<b>0.9010</b>	<b>32.54</b>	<b>0.9320</b>	<b>39.25</b>	<b>0.9783</b>
Bicubic	$\times 3$	-	-	30.39	0.8682	27.55	0.7742	27.21	0.7385	24.46	0.7349	26.95	0.8556
SRCNN[6]	$\times 3$	<b>57K</b>	52.7G	32.75	0.9090	29.30	0.8215	28.41	0.7863	26.24	0.7989	30.48	0.9117
VDNR[23]	$\times 3$	665K	612.6G	33.67	0.9210	29.78	0.8320	28.83	0.7990	27.14	0.8290	32.01	0.9340
DRCN[24]	$\times 3$	1774K	9788.7G	33.82	0.9226	29.76	0.8311	28.80	0.7963	27.14	0.8279	32.24	0.9343
DRRN[42]	$\times 3$	297K	6797.0G	34.03	0.9244	29.96	0.8349	28.95	0.8004	27.53	0.8378	32.74	0.9390
MemNet[43]	$\times 3$	677K	623.9G	34.09	0.9248	30.01	0.8350	28.96	0.8001	27.56	0.8376	32.51	0.9369
CARN[1]	$\times 3$	1592K	118.8G	34.29	0.9255	30.29	0.8407	29.06	0.8034	28.06	0.8493	33.50	0.9440
IDN[17]	$\times 3$	553K	57.0G	34.11	0.9253	29.99	0.8354	28.95	0.8013	27.42	0.8359	32.71	0.9381
SRFBN-S[28]	$\times 3$	375K	686.4G	34.20	0.9255	30.10	0.8372	28.96	0.8010	27.66	0.8415	33.02	0.9404
IMDN[16]	$\times 3$	703K	71.5G	34.36	0.9270	30.32	0.8417	29.09	0.8046	28.17	0.8519	33.61	0.9445
LatticeNet[31]	$\times 3$	765K	76.3G	34.53	0.9281	30.39	0.8424	29.15	0.8059	28.33	0.8538	-	-
SMSR[48]	$\times 3$	993K	67.8G	34.40	0.9270	30.33	0.8412	29.10	0.8050	28.25	0.8536	33.68	0.9445
HPUN-S	$\times 3$	<u>234K</u>	<b>21.3G</b>	34.32	0.9262	30.25	0.8404	29.05	0.8036	27.80	0.8456	33.31	0.9425
HPUN-M	$\times 3$	500K	48.1G	34.39	0.9269	30.33	0.8420	29.11	0.8052	28.06	0.8508	33.54	0.9441
HPUN-L	$\times 3$	723K	69.3G	<b>34.56</b>	<b>0.9281</b>	<b>30.45</b>	<b>0.8445</b>	<b>29.18</b>	<b>0.8072</b>	<b>28.37</b>	<b>0.8572</b>	<b>33.90</b>	<b>0.9463</b>
HPUN-S+	$\times 3$	<u>234K</u>	<b>21.3G</b>	34.39	0.9269	30.33	0.8417	29.09	0.8046	27.92	0.8477	33.58	0.9441
HPUN-M+	$\times 3$	500K	<u>48.1G</u>	34.47	0.9276	30.41	0.8432	29.15	0.8060	28.18	0.8529	33.81	0.9457
HPUN-L+	$\times 3$	723K	69.3G	<b>34.63</b>	<b>0.9287</b>	<b>30.52</b>	<b>0.8455</b>	<b>29.22</b>	<b>0.8080</b>	<b>28.49</b>	<b>0.8592</b>	<b>34.12</b>	<b>0.9476</b>
Bicubic	$\times 4$	-	-	28.42	0.8104	26.00	0.7027	25.96	0.6675	23.14	0.6577	24.89	0.7866
SRCNN[6]	$\times 4$	<b>57K</b>	52.7G	30.48	0.8628	27.50	0.7513	26.90	0.7101	24.52	0.7221	27.58	0.8555
VDNR[23]	$\times 4$	665K	612.6G	31.35	0.8830	28.02	0.7680	27.29	0.7260	25.18	0.7540	28.83	0.8870
DRCN[24]	$\times 4$	1774K	9788.7G	31.53	0.8854	28.02	0.7670	27.23	0.7233	25.18	0.7524	28.93	0.8854
DRRN[42]	$\times 4$	297K	6797.0G	31.68	0.8888	28.21	0.7720	27.38	0.7284	25.44	0.7638	29.46	0.8960
LapSRN[26]	$\times 4$	813K	149.4G	31.54	0.8850	28.19	0.7720	27.32	0.7280	25.21	0.7560	29.09	0.8845
MemNet[43]	$\times 4$	677K	623.9G	31.74	0.8893	28.26	0.7723	27.40	0.7281	25.50	0.7630	29.42	0.8942
CARN[1]	$\times 4$	1592K	90.9G	32.13	0.8937	28.60	0.7806	27.58	0.7349	26.07	0.7837	30.47	0.9084
IDN[17]	$\times 4$	553K	32.3G	31.82	0.8903	28.25	0.7730	27.41	0.7297	25.41	0.7632	29.41	0.8942
SRFBN-S[28]	$\times 4$	483K	852.9G	31.98	0.8923	28.45	0.7779	27.44	0.7313	25.71	0.7719	29.91	0.9008
IMDN[16]	$\times 4$	715K	40.9G	32.21	0.8948	28.58	0.7811	27.56	0.7353	26.04	0.7838	30.45	0.9075
LatticeNet[31]	$\times 4$	777K	43.6G	32.30	0.8962	28.68	0.7830	27.62	0.7367	26.25	0.7873	-	-
SMSR[48]	$\times 4$	1006K	41.6G	32.12	0.8932	28.55	0.7808	27.55	0.7351	26.11	0.7868	30.54	0.9085
HPUN-S	$\times 4$	<u>246K</u>	<b>12.7G</b>	32.00	0.8921	28.50	0.7792	27.51	0.7339	25.79	0.7769	30.14	0.9038
HPUN-M	$\times 4$	511K	<u>27.7G</u>	32.19	0.8946	28.61	0.7818	27.58	0.7364	26.04	0.7851	30.49	0.9078
HPUN-L	$\times 4$	734K	39.7G	<b>32.31</b>	<b>0.8962</b>	<b>28.73</b>	<b>0.7842</b>	<b>27.66</b>	<b>0.7386</b>	<b>26.27</b>	<b>0.7918</b>	<b>30.77</b>	<b>0.9109</b>
HPUN-S+	$\times 4$	<u>246K</u>	<b>12.7G</b>	32.14	0.8940	28.60	0.7808	27.56	0.7350	25.90	0.7796	30.43	0.9070
HPUN-M+	$\times 4$	511K	<u>27.7G</u>	32.29	0.8959	28.69	0.7833	27.64	0.7377	26.15	0.7877	30.74	0.9106
HPUN-L+	$\times 4$	734K	39.7G	<b>32.40</b>	<b>0.8974</b>	<b>28.80</b>	<b>0.7856</b>	<b>27.70</b>	<b>0.7397</b>	<b>26.38</b>	<b>0.7943</b>	<b>31.00</b>	<b>0.9133</b>

is higher. Although our HPUN-L cannot catch up with the LatticeNet [31] On Set5 dataset with the scale of  $\times 2$ , its computation costs and parameters are smaller. The results of HPUN-L+ show that we can further improve the performance with self-ensemble technique.

Our HPUN-M network can achieve top-3 performance on Set14 and B100 for each scale. Besides, compared with other competitive methods such as IMDN [16],



**Table 4.** We compare the storage size (KB) and inference time (ms) for real-world test. The results are generated on Set5 with scale  $\times 2$ .

Methods	PSNR(Set5)	Size	Inference Time
EDSR Baseline [29]	38.05	5366KB	460ms
HPUN-L	38.09	2858KB	240ms
HPUN-M	38.03	1902KB	176ms
HPUN-S	37.93	904KB	162ms

LatticeNet [31], and SMSR [48], it only has two thirds or even fewer parameters and Multi-Adds. Moreover, it can achieve top-5 performance on each dataset with any scale. Furthermore, we can significantly improve the HPUN-M network using the self-ensemble technique. Our HPUN-S achieve comparable performance with the second least parameters among all the methods. When the scale is set to  $\times 3$  and  $\times 4$ , it takes the minor computation costs among all the methods.

We specifically compare the HPUN-S network with the SRFBN-S[28] and CARN [1], since SRFBN-S also uses the low-frequency features to enhance the inference features and CARN implements group convolutions for the lightweight purpose as well. As shown from the table, our HPUN-S network can achieve around 0.08dB than SRFBN-S on the PSNR of Set5 on average. In the meanwhile, the parameters and Multi-Adds of the HPUN-S network are 64.4% and 4.2%, respectively. The comparisons show that our proposed module can significantly improve the SR performance using low-resolution features without any complicated operations. Compared with CARN, our model achieves better PSNR when the scale is  $\times 2$  and  $\times 3$  with 14.8% and 17.9% of its size and Multi-Adds. **Inference Time.** We also show the real-world results besides the theoretical evaluation. The results are shown in the Table 4. From the table we find out that the speed of HPUN-S is not as much faster as the theoretical calculation comparing with the HPUN-M. This may be caused by the better optimization of standard convolution on CUDA. We believe that HPUN-S can be faster in the environment specified for edge devices.

**Visualization Results.** Visualization results are shown in Figure 10. The results are generated with  $\times 4$  scale on Urban100 and Manga109. Compared with other methods, our HPUN-L network generates better reconstruction results, especially on Manga109. As shown in the figure, the results of our HPUN-L network have fewer artifacts than other methods.

## 5 Conclusions

In this paper, we proposed a lightweight network named Hybrid Pixel-Unshuffled Network (HPUN) for image SR. Specifically, we design the Self-Residual Depth-wise Separable Convolution to overcome the defects of the depthwise convolution, and the pixel-unshuffled downsampling to enhance the performance with low-frequency representations. Both proposed modules take limited computation costs and parameters. With the two proposed modules, we design a lightweight block named Hybrid Pixel-Unshuffled Block with the standard convolution layer

and the proposed Pixel-Unshuffled Block. The HPUN can achieve new SOTA performance with limited parameters and Multi-Adds. We also discover and discuss the relationship between the PSNR and the NME among the shallow features and deep features. We believe that the phenomenon should be general, and we can take advantage of it for network design.

## References

1. Namhyuk Ahn, Byungkun Kang, and Kyung-Ah Sohn. Fast, accurate, and lightweight super-resolution with cascading residual network. In *ECCV*, 2018.
2. Marco Bevilacqua, Aline Roumy, Christine Guillemot, and Marie Line Alberi-Morel. Low-complexity single-image super-resolution based on nonnegative neighbor embedding. In *BMVC*, 2012.
3. Han Cai, Ligeng Zhu, and Song Han. Proxylessnas: Direct neural architecture search on target task and hardware. In *ICLR*, 2019.
4. Francois Chollet. Xception: Deep learning with depthwise separable convolutions. In *CVPR*, 2017.
5. Chao Dong, Chen Change Loy, Kaiming He, and Xiaoou Tang. Learning a deep convolutional network for image super-resolution. In *ECCV*, 2014.
6. Chao Dong, Chen Change Loy, Kaiming He, and Xiaoou Tang. Image super-resolution using deep convolutional networks. *TPAMI*, 2016.
7. Chao Dong, Chen Change Loy, and Xiaoou Tang. Accelerating the super-resolution convolutional neural network. In *ECCV*, 2016.
8. Xavier Glorot, Antoine Bordes, and Yoshua Bengio. Deep sparse rectifier neural networks. In *AISTATS*, 2011.
9. Kai Han, Yunhe Wang, Qi Tian, Jianyuan Guo, Chunjing Xu, and Chang Xu. Ghostnet: More features from cheap operations. In *CVPR*, 2020.
10. Song Han, Jeff Pool, John Tran, and William J Dally. Learning both weights and connections for efficient neural network. In *NeurIPS*, 2015.
11. Muhammad Haris, Gregory Shakhnarovich, and Norimichi Ukita. Deep back-projection networks for super-resolution. In *CVPR*, 2018.
12. Andrew Howard, Mark Sandler, Grace Chu, Liang-Chieh Chen, Bo Chen, Mingxing Tan, Weijun Wang, Yukun Zhu, Ruoming Pang, Vijay Vasudevan, et al. Searching for mobilenetv3. In *ICCV*, 2019.
13. Andrew G Howard, Menglong Zhu, Bo Chen, Dmitry Kalenichenko, Weijun Wang, Tobias Weyand, Marco Andreetto, and Hartwig Adam. Mobilenets: Efficient convolutional neural networks for mobile vision applications. *CoRR*, abs/1704.04861, 2017.
14. Gao Huang, Shichen Liu, Laurens van der Maaten, and Kilian Q. Weinberger. Condensenet: An efficient densenet using learned group convolutions. In *CVPR*, June 2018.
15. Jia-Bin Huang, Abhishek Singh, and Narendra Ahuja. Single image super-resolution from transformed self-exemplars. In *CVPR*, 2015.
16. Zheng Hui, Xinbo Gao, Yunchu Yang, and Xiumei Wang. Lightweight image super-resolution with information multi-distillation network. In *ACMMM*, 2019.
17. Zheng Hui, Xiumei Wang, and Xinbo Gao. Fast and accurate single image super-resolution via information distillation network. In *CVPR*, 2018.
18. Forrest N Iandola, Song Han, Matthew W Moskewicz, Khalid Ashraf, William J Dally, and Kurt Keutzer. Squeezenet: Alexnet-level accuracy with 50x fewer parameters and 0.5 mb model size. *ICLR*, 2017.

19. Sergey Ioffe and Christian Szegedy. Batch normalization: Accelerating deep network training by reducing internal covariate shift. In *ICML*, 2015.
20. Jonghoon Jin, Aysegul Dundar, and Eugenio Culurciello. Flattened convolutional neural networks for feedforward acceleration. *CoRR*, 2014.
21. Mingxing JTan and Quoc V Le. Mixnet: Mixed depthwise convolutional kernels. In *BMVC*, 2019.
22. Tero Karras, Timo Aila, Samuli Laine, and Jaakko Lehtinen. Progressive growing of gans for improved quality, stability, and variation. *submitted to ICLR 2018*, 2017.
23. Jiwon Kim, Jung Kwon Lee, and Kyoung Mu Lee. Accurate image super-resolution using very deep convolutional networks. In *CVPR*, 2016.
24. Jiwon Kim, Jung Kwon Lee, and Kyoung Mu Lee. Deeply-recursive convolutional network for image super-resolution. In *CVPR*, 2016.
25. Diederik Kingma and Jimmy Ba. Adam: A method for stochastic optimization. In *ICLR*, 2015.
26. Wei-Sheng Lai, Jia-Bin Huang, Narendra Ahuja, and Ming-Hsuan Yang. Deep laplacian pyramid networks for fast and accurate super-resolution. In *CVPR*, 2017.
27. Christian Ledig, Lucas Theis, Ferenc Huszár, Jose Caballero, Andrew Cunningham, Alejandro Acosta, Andrew Aitken, Alykhan Tejani, Johannes Totz, Zehan Wang, and Wenzhe Shi. Photo-realistic single image super-resolution using a generative adversarial network. In *CVPR*, 2017.
28. Zhen Li, Jinglei Yang, Zheng Liu, Xiaomin Yang, Gwanggil Jeon, and Wei Wu. Feedback network for image super-resolution. In *CVPR*, 2019.
29. Bee Lim, Sanghyun Son, Heewon Kim, Seungjun Nah, and Kyoung Mu Lee. Enhanced deep residual networks for single image super-resolution. In *CVPRW*, 2017.
30. Hanxiao Liu, Karen Simonyan, and Yiming Yang. Darts: Differentiable architecture search. In *ICLR*, 2019.
31. Xiaotong Luo, Yuan Xie, Yulun Zhang, Yanyun Qu, Cuihua Li, and Yun Fu. Latticenet: Towards lightweight image super-resolution with lattice block. In *ECCV*, 2020.
32. Ningning Ma, Xiangyu Zhang, Hai-Tao Zheng, and Jian Sun. Shufflenet v2: Practical guidelines for efficient cnn architecture design. In *ECCV*, 2018.
33. David Martin, Charless Fowlkes, Doron Tal, and Jitendra Malik. A database of human segmented natural images and its application to evaluating segmentation algorithms and measuring ecological statistics. In *ICCV*, 2001.
34. Yusuke Matsui, Kota Ito, Yuji Aramaki, Azuma Fujimoto, Toru Ogawa, Toshihiko Yamasaki, and Kiyoharu Aizawa. Sketch-based manga retrieval using manga109 dataset. *Multimedia Tools and Applications*, 2017.
35. Adam Paszke, Sam Gross, Francisco Massa, Adam Lerer, James Bradbury, Gregory Chanan, Trevor Killeen, Zeming Lin, Natalia Gimeshein, Luca Antiga, et al. Pytorch: An imperative style, high-performance deep learning library. In *NeurIPS*, 2019.
36. Mark Sandler, Andrew Howard, Menglong Zhu, Andrey Zhmoginov, and Liang-Chieh Chen. Inverted residuals and linear bottlenecks: Mobile networks for classification, detection and segmentation. *CVPR*, 2018.
37. Samuel Schulter, Christian Leistner, and Horst Bischof. Fast and accurate image upscaling with super-resolution forests. In *CVPR*, 2015.
38. Wenzhe Shi, Jose Caballero, Ferenc Huszár, Johannes Totz, Andrew P Aitken, Rob Bishop, Daniel Rueckert, and Zehan Wang. Real-time single image and video super-resolution using an efficient sub-pixel convolutional neural network. In *CVPR*, 2016.



39. Wenzhe Shi, Jose Caballero, Christian Ledig, Xiahai Zhuang, Wenjia Bai, Kanwal Bhatia, Antonio M Simoes Monteiro de Marvao, Tim Dawes, Declan O'Regan, and Daniel Rueckert. Cardiac image super-resolution with global correspondence using multi-atlas patchmatch. In *MICCAI*, 2013.
40. Laurent Sifre and PS Mallat. *Rigid-motion scattering for image classification*. PhD thesis, Citeseer, 2014.
41. Ke Sun, Bin Xiao, Dong Liu, and Jingdong Wang. Deep high-resolution representation learning for human pose estimation. In *CVPR*, 2019.
42. Ying Tai, Jian Yang, and Xiaoming Liu. Image super-resolution via deep recursive residual network. In *CVPR*, 2017.
43. Ying Tai, Jian Yang, Xiaoming Liu, and Chunyan Xu. Memnet: A persistent memory network for image restoration. In *ICCV*, 2017.
44. Mingxing Tan and Quoc Le. Efficientnet: Rethinking model scaling for convolutional neural networks. In *ICML*, 2019.
45. Radu Timofte, Eirikur Agustsson, Luc Van Gool, Ming-Hsuan Yang, Lei Zhang, Bee Lim, Sanghyun Son, Heewon Kim, Seungjun Nah, Kyoung Mu Lee, et al. Ntire 2017 challenge on single image super-resolution: Methods and results. In *CVPRW*, 2017.
46. Tong Tong, Gen Li, Xiejie Liu, and Qinquan Gao. Image super-resolution using dense skip connections. In *ICCV*, 2017.
47. Jingdong Wang, Ke Sun, Tianheng Cheng, Borui Jiang, Chaorui Deng, Yang Zhao, Dong Liu, Yadong Mu, Mingkui Tan, Xinggang Wang, et al. Deep high-resolution representation learning for visual recognition. *IEEE transactions on pattern analysis and machine intelligence*, 43(10):3349–3364, 2020.
48. Longguang Wang, Xiaoyu Dong, Yingqian Wang, Xinyi Ying, Zaiping Lin, Wei An, and Yulan Guo. Exploring sparsity in image super-resolution for efficient inference. In *CVPR*, 2021.
49. Longguang Wang, Xiaoyu Dong, Yingqian Wang, Xinyi Ying, Zaiping Lin, Wei An, and Yulan Guo. Exploring sparsity in image super-resolution for efficient inference. In *CVPR*, 2021.
50. Zhou Wang, Alan C Bovik, Hamid R Sheikh, and Eero P Simoncelli. Image quality assessment: from error visibility to structural similarity. *TIP*, 2004.
51. Bichen Wu, Xiaoliang Dai, Peizhao Zhang, Yanghan Wang, Fei Sun, Yiming Wu, Yuandong Tian, Peter Vajda, Yangqing Jia, and Kurt Keutzer. Fbnet: Hardware-aware efficient convnet design via differentiable neural architecture search. In *CVPR*, 2019.
52. Yu Yin, Joseph P Robinson, Songyao Jiang, Yue Bai, Can Qin, and Yun Fu. Superfront: From low-resolution to high-resolution frontal face synthesis. In *ACMMM*, 2021.
53. Yu Yin, Joseph P Robinson, Yulun Zhang, and Yun Fu. Joint super-resolution and alignment of tiny faces. In *AAAI*, 2020.
54. Roman Zeyde, Michael Elad, and Matan Protter. On single image scale-up using sparse-representations. In *Proc. 7th Int. Conf. Curves Surf.*, 2010.
55. He Zhang and Vishal M Patel. Densely connected pyramid dehazing network. In *CVPR*, 2018.
56. Ke Zhang, Miao Sun, Xu Han, Xingfang Yuan, Liru Guo, and Tao Liu. Residual networks of residual networks: Multilevel residual networks. *TCSVT*, 2017.
57. Kai Zhang, Wangmeng Zuo, Shuhang Gu, and Lei Zhang. Learning deep cnn denoiser prior for image restoration. In *CVPR*, 2017.
58. Kai Zhang, Wangmeng Zuo, and Lei Zhang. Learning a single convolutional super-resolution network for multiple degradations. In *CVPR*, 2018.

- 59. Xiangyu Zhang, Xinyu Zhou, Mengxiao Lin, and Jian Sun. Shufflenet: An extremely efficient convolutional neural network for mobile devices. In *CVPR*, 2018.
- 60. Yulun Zhang, Kunpeng Li, Kai Li, Lichen Wang, Bineng Zhong, and Yun Fu. Image super-resolution using very deep residual channel attention networks. In *ECCV*, 2018.
- 61. Yulun Zhang, Kunpeng Li, Kai Li, Bineng Zhong, and Yun Fu. Residual non-local attention networks for image restoration. In *ICLR*, 2019.
- 62. Yulun Zhang, Yapeng Tian, Yu Kong, Bineng Zhong, and Yun Fu. Residual dense network for image super-resolution. In *CVPR*, 2018.
- 63. Barret Zoph, Vijay Vasudevan, Jonathon Shlens, and Quoc V Le. Learning transferable architectures for scalable image recognition. In *CVPR*, 2018.
- 64. Wilman WW Zou and Pong C Yuen. Very low resolution face recognition problem. *TIP*, 2012.